

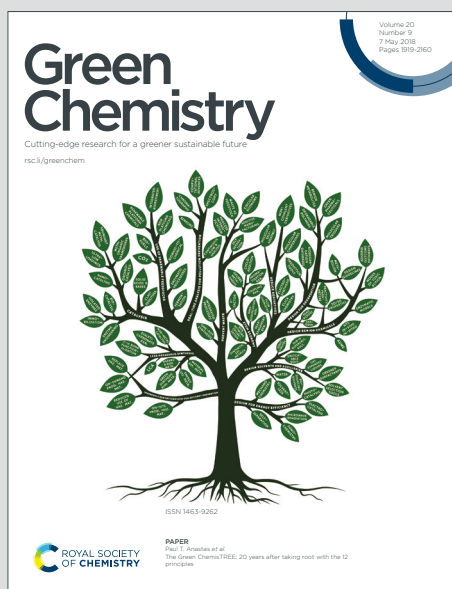
# Green Chemistry

Cutting-edge research for a greener sustainable future

Accepted Manuscript

View Article Online  
View Journal

This article can be cited before page numbers have been issued, to do this please use: X. Ge, G. Delmonache, S. Prakash, M. Janpandit, P. Gogoi, Z. Li and Y. Li, *Green Chem.*, 2026, DOI: 10.1039/D5GC05361G.



This is an Accepted Manuscript, which has been through the Royal Society of Chemistry peer review process and has been accepted for publication.

Accepted Manuscripts are published online shortly after acceptance, before technical editing, formatting and proof reading. Using this free service, authors can make their results available to the community, in citable form, before we publish the edited article. We will replace this Accepted Manuscript with the edited and formatted Advance Article as soon as it is available.

You can find more information about Accepted Manuscripts in the [Information for Authors](#).

Please note that technical editing may introduce minor changes to the text and/or graphics, which may alter content. The journal's standard [Terms & Conditions](#) and the [Ethical guidelines](#) still apply. In no event shall the Royal Society of Chemistry be held responsible for any errors or omissions in this Accepted Manuscript or any consequences arising from the use of any information it contains.

## Green Foundation

1. This work illustrated a new approach for the direct valorization of bicarbonate capture solution to ethylene. This approach simplifies two separate carbon capture and conversion steps and operates at ambient conditions completely, thereby minimizing both environmental impacts and energy consumption.
2. A Faradaic efficiency of 83.7% to C<sub>2</sub>+ products was achieved at -200 mA cm<sup>-2</sup> with 59.5% ethylene selectivity - one of the highest performances for the direct conversion of bicarbonate to ethylene.
3. Future work will explore further improving energy efficiency and production throughput of the system. Technoeconomic analysis can be conducted to identify pinch point of the system.



## ARTICLE

## Direct Conversion of Bicarbonate Capture Solution to Multi-carbon Products in a Plasma Electrochemical System

Xiaoli Ge,<sup>a</sup> Gina DelMonache,<sup>a</sup> Shwetha Prakash,<sup>a</sup> Mayuresh Janpandit,<sup>a</sup> Pratahdeep Gogoi,<sup>a</sup> Zhaoqiang Li,<sup>b</sup> and Yuguang C. Li<sup>\*a</sup>Received 00th January 20xx,  
Accepted 00th January 20xx

DOI: 10.1039/x0xx00000x

Atmospheric CO<sub>2</sub> capture has become an increasingly important industrial process in response to climate challenges. Conventional CO<sub>2</sub> capture processes often require an energy-intensive step to regenerate the capture solution, typically a (bi)carbonate solution. Developing new chemical processes that directly convert the capture solution can bypass this energy-demanding regeneration step and yield valuable multi-carbon products. This study introduces a hybrid nonthermal plasma-electrochemical system that enables the direct conversion of bicarbonate molecules into ethylene with high yield. The captured bicarbonate solution is activated directly by solvated electrons and radical species generated from the plasma. The effects of counter cations in the HCO<sub>3</sub><sup>-</sup> solution and carrier gas in the plasma reactor on the composition of plasma-activated intermediates, including O<sub>2</sub>, H<sub>2</sub>, CO, CO<sub>2</sub>, and CH<sub>4</sub>, were examined using NMR and GC/MS analyses. These mixed plasma-activated gaseous products, containing up to 73.5 vol% CO and CO<sub>2</sub>, were subsequently introduced into an electrolyzer, achieving an 83.7% C<sub>2</sub><sup>+</sup> Faradaic efficiency at 200 mA cm<sup>-2</sup> with 59.5% ethylene selectivity. This approach demonstrates the direct transformation of carbon capture solutions into high-yield C<sub>2</sub><sup>+</sup> products and establishes a platform for the chemical activation of otherwise inert molecules.

## 1. Introduction

As global CO<sub>2</sub> level continue to rise due to industrial and human activities, environmental problems and energy crises are an ever pressing problem for our society.<sup>1-3</sup> Therefore, capturing and converting atmospheric CO<sub>2</sub> into high-value chemicals has become a critical research area.<sup>4</sup> The electrochemical reduction of carbon dioxide, powered by renewable electricity, provides a promising approach to realizing carbon neutrality while generating highly valuable products and fuels, such as ethylene and ethanol.<sup>5</sup> However, industrial-scale CO<sub>2</sub> electrolyzers, despite their efficiency, require a high-purity CO<sub>2</sub> stream, which typically comes from CO<sub>2</sub> capture from air or an industrial flue gas stream. These processes demand significant energy input, especially for CO<sub>2</sub> regeneration like the drying and calcination processes.<sup>4, 6</sup>

Considering the energy consumption, researchers are exploring strategies to directly couple upstream CO<sub>2</sub> capture with a CO<sub>2</sub> conversion device, realizing in situ CO<sub>2</sub> regeneration and conversion from CO<sub>2</sub> capture products, such as bicarbonate or carbonate solution.<sup>7-9</sup> Compared with a gas-fed CO<sub>2</sub> electrolyzer, a liquid-fed (bi)carbonate electrolyzer can

significantly reduce the system complexity and approach high CO<sub>2</sub> utilization. Li et al. developed a bipolar membrane (BPM)-membrane electrode assembly (MEA) system that can convert carbonate solution directly to produce pure syngas with a ca. 3:1 H<sub>2</sub>:CO ratio and achieve 100% carbon utilization from the carbonate solution.<sup>10</sup> This device operates based on the reaction between the proton generated from BPM and the carbonate solution to produce CO<sub>2</sub> in situ locally on the catalyst's surface. Several follow-up studies have since investigated the influence of the BPM, interlayer, or catalyst designs on the local pH with the goal of increasing the in situ generated CO<sub>2</sub>.<sup>11-13</sup> The Hatzell group demonstrated a Ni-based single-atom electrocatalyst integrated with a BPM-MEA to directly convert bicarbonate into CO, achieving a 93% CO FE.<sup>12</sup> However, these (bi)carbonate electrolyzers still face some limitations. First, their selectivity for C<sub>2</sub><sup>+</sup> products is typically lower compared to conventional CO<sub>2</sub>RR electrolyzers due to the low CO<sub>2</sub> concentration on the catalyst surface. Second, (bi)carbonate electrolyzers require a BPM or a cation exchange membrane (CEM) to generate or transport H<sup>+</sup> for CO<sub>2</sub> generation, which can increase the rate of the competing hydrogen evolution reaction. From a practical perspective, the water dissociation within the BPM and the thickness of the BPM may lead to a high overall cell voltage, which could pose a challenge for scaling up. To continue advancing the field of direct bicarbonate conversion to value-added chemicals, new methods of activating bicarbonate solutions are needed.

In recent years, researchers have demonstrated the applications of non-thermal plasma technology in a number of

<sup>a</sup> Department of Chemistry, University at Buffalo, State University of New York, Buffalo, New York, 14260, USA. Email: yuguangl@buffalo.edu

<sup>b</sup> Department of Physics, Faculty of Arts and Sciences, Beijing Normal University, Zhuhai, Guangdong, 519087, P.R. China.

Supplementary Information available: Materials synthesis and characterization, plasma reactor design, electrochemical experiments, Fig. S1–S12, and Tables S1–S6. See DOI: 10.1039/x0xx00000x



different catalysis reactions under ambient conditions.<sup>14-16</sup> Non-thermal plasma or room temperature plasma is typically generated via a dielectric barrier discharge mechanism and it can activate thermodynamically stable molecules like CO<sub>2</sub> or N<sub>2</sub> into reactive species, allowing subsequent conversion into value-added compounds. For example, plasma conversion has been demonstrated by activating CH<sub>4</sub> or H<sub>2</sub> alongside CO<sub>2</sub> to generate hydrocarbons.<sup>17-20</sup> While plasma chemistry provides sufficient energy to break up any chemical bonds, reaction selectivity control is often very difficult. Therefore, incorporating catalysts into plasma reactors has been an ongoing research area to stabilize and facilitate the binding of reactants to steer the reaction outcome.<sup>17, 18, 20</sup> The continued development of plasma catalysis, especially in the direction of controlling reaction selectivity, could bring significant breakthroughs for catalysis science. Given the success of plasma CO<sub>2</sub> catalytic conversion, we posit that bicarbonate molecules, which are similar to CO<sub>2</sub> molecules, could also be activated via plasma and enable a new approach for direct bicarbonate solution conversion into value-added chemicals.

This work presents, for the first time, a new approach for coupling the plasma reactor with an electrolyzer to realize the reduction of plasma-activated bicarbonate, overcoming the limitations of in situ generated CO<sub>2</sub> concentration in the BPM bicarbonate electrolyzer. We employ a cascading plasma-electrochemical approach where the plasma reactor activates the bicarbonate solution, and the electrochemical reactor steers the reaction outcome with an optimally designed catalyst. This approach allows us to control separately the activation of bicarbonate and its reaction selectivity. In the plasma reactor, the bicarbonate solution was activated into H<sub>2</sub>, O<sub>2</sub>, CH<sub>4</sub>, and CO<sub>2</sub>, which were then used in CO<sub>2</sub>RR. The mechanism of HCO<sub>3</sub><sup>-</sup> activation in the solution phase vs. gas phase concentration was investigated by studying the effects of concentration, cations paired with HCO<sub>3</sub><sup>-</sup> and the carrier gas in the plasma reactor on the composition of plasma-activated products. Under optimized plasma conditions, our continuous plasma-electrochemical system with a tandem electrocatalyst CuAg achieved a total C<sub>2+</sub> FE of 83.7% at 200 mA cm<sup>-2</sup>. To the best of our knowledge, this is one of the highest FE for the direct conversion of bicarbonate solutions to C<sub>2+</sub> products. These results highlight the potential of our plasma-electrochemical approach to separately control the reaction activation and selectivity of thermodynamically stable chemicals, enabling new pathways for other chemical transformations, such as methane oxidation or plastic upcycling.

## 2. Experimental

All chemicals were directly used as received without further purification. The anion exchange membrane (AEM) was purchased from the Fuel Cell Store. Potassium hydroxide (KOH), potassium bicarbonate (KHCO<sub>3</sub>), and silver nitrate (AgNO<sub>3</sub>) were obtained from Thermo Scientific. Ni foam was purchased from MTI Corporation.

### Catalyst preparation

The Cu catalyst was prepared by sputtering a ~250 nm Cu layer on a polytetrafluoroethylene (PTFE) membrane using the Kurt J. Lesker Company PRO Line PVD 75. The CuAg bimetallic catalyst was synthesized by a galvanic exchange method. A piece of Cu-PTFE was immersed in 5 mL of a 5 mM AgNO<sub>3</sub> solution for 5 minutes at room temperature and then rinsed with deionized (DI) water and air dried.

### Materials characterization

Scanning electron microscopy (SEM) and energy-dispersive X-ray spectroscopy (EDS) images were obtained by the Carl Zeiss AURIGA CrossBeam. The surface compositions were analyzed using X-ray photoelectron spectroscopy (XPS) with a PHI 5000 Versaprobe. Mass spectra were acquired using an Agilent 6890 series gas chromatography system coupled with a 5973 mass selective detector. The <sup>1</sup>H-NMR spectra were recorded using a Bruker 500 MHz system. Gas products were analyzed using gas chromatography (PerkinElmer, Clarus 590 GC) equipped with Carboxen 1000 and Mol Sieve 5A columns.

To evaluate the radical formation under different cation electrolyte, 10 mM 2,2,6,6-Tetramethylpiperidine 1-oxyl (TEMPO) was added to the plasma reactor under typical operation condition. The concentration of the radicals generated from plasma was extracted from electron spin resonance spectroscopy.

### Plasma reactor design

Our custom-made plasma reactor consists of a glass bottle as the main container, a saturated KHCO<sub>3</sub> solution as the reactant, a copper rod as the high-voltage electrode, and a nickel foam as the ground electrode. Voltage profile of plasma was measured with an oscilloscope and a high voltage probe.

### Electrochemical experiments

A 1.0 M KOH was used as both catholyte and anolyte and circulated with a peristaltic pump. The prepared Cu/CuAg-PTFE catalysts were applied as the cathode, Ni foam as the anode, and Ag/AgCl as the reference electrode. An anion exchange membrane (AEM) was placed between the anode and cathode. Electrochemical measurements were conducted using a SquidstatPlus Potentiostat (Admiral Instruments) in a flow cell. CO<sub>2</sub>RR was performed at current densities of -100, -200, -300, and -400 mA cm<sup>-2</sup>. Different carrier gases from the plasma reactor were used as the inlet.

For the plasma production rate calculation (Fig. 2c-f, S6 and S7), the H<sub>2</sub> and O<sub>2</sub> from the carrier gas were first subtracted. The inlet CO<sub>2</sub>RR stream (the outlet of the plasma reactor) consists of a mixture of CO<sub>2</sub>, CO, O<sub>2</sub>, CH<sub>4</sub>, and H<sub>2</sub>, some of which are also products of the CO<sub>2</sub>RR. The FE reported in Fig. 3, 4, S12 are calculated by subtracting the contributions of CO, CH<sub>4</sub>, and H<sub>2</sub> from the plasma reaction—more specifically—GC measurements were conducted before every electrochemical CO<sub>2</sub>RR to determine the amount of CO, CH<sub>4</sub>, and H<sub>2</sub> from the plasma reaction. The CO, CH<sub>4</sub>, and H<sub>2</sub> contributions from plasma are subtracted from the CO<sub>2</sub>RR results to calculate the FE. For the stability test, a constant current density of -200 mA cm<sup>-2</sup> was applied. The jV curves were obtained through chronoamperometry experiments at different voltages for 5 minutes. The current densities averaged stable values in the final minute. All experiments were conducted in triplicate.



## 3. Results and discussion

added a glass tube container around the copper electrode to

DOI: 10.1039/D5GC05361G

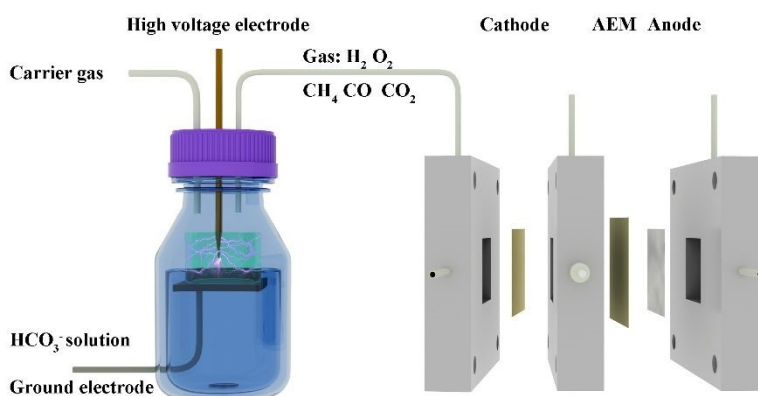


**Fig. 1.** Illustration of a continuous-flow plasma electrochemical setup for bicarbonate activation. Bicarbonate ions are first activated in solution form,  $\text{CO}_2$  is generated and then converted into ethylene in the subsequent electrochemical reactor.

The plasma-electrochemical system setup is illustrated in Fig. 1. Our custom plasma reactor is based on a dielectric barrier discharge mechanism and it is modified from previous reports.<sup>21-23</sup> A copper nail is used as the high-voltage electrode, while a nickel foam acts as the ground electrode, facilitating plasma discharge at the  $\text{HCO}_3^-$  solution interface. The plasma-activated gas products were then purged into the flow cell for  $\text{CO}_2$ RR. To maintain a stable flow rate for  $\text{CO}_2$ RR, a carrier gas at 5 sccm was used to purge the plasma reactor bottle into the electrochemical reactor. As illustrated in Fig. S1a-c, during a plasma strike, visible vapor is generated inside the bottle. These vapors lead to plasma discharge in random orientation due to the water droplet next to the copper electrode creating a path for discharge. To maintain a consistent plasma output, we

constrain the plasma strikes, making them more concentrated towards the solution surface (Fig. S1d-f). Gas chromatography-mass spectrometry (GC-MS) and  $^1\text{H}$  nuclear magnetic resonance (NMR) spectroscopy were applied to qualitatively identify the plasma-activated carbonaceous reactants in the gas and liquid phase, respectively. As shown in Fig. 2a and Fig. S2-3,  $\text{O}_2$ ,  $\text{CO}$ ,  $\text{CO}_2$ , and  $\text{CH}_4$  were detected with GC-MS.  $\text{H}_2$  was also detected with GC equipped with an FID detector (Fig. S2). These initial results confirm that plasma can efficiently activate the  $\text{HCO}_3^-$  molecule into smaller fragments. A plasma-electrochemical scheme will be a viable approach for the direct conversion of bicarbonate to value-added products. Given the plasma discharge at the  $\text{HCO}_3^-$  solution interface, the bicarbonate solution inside the plasma reactor was analyzed and methanol

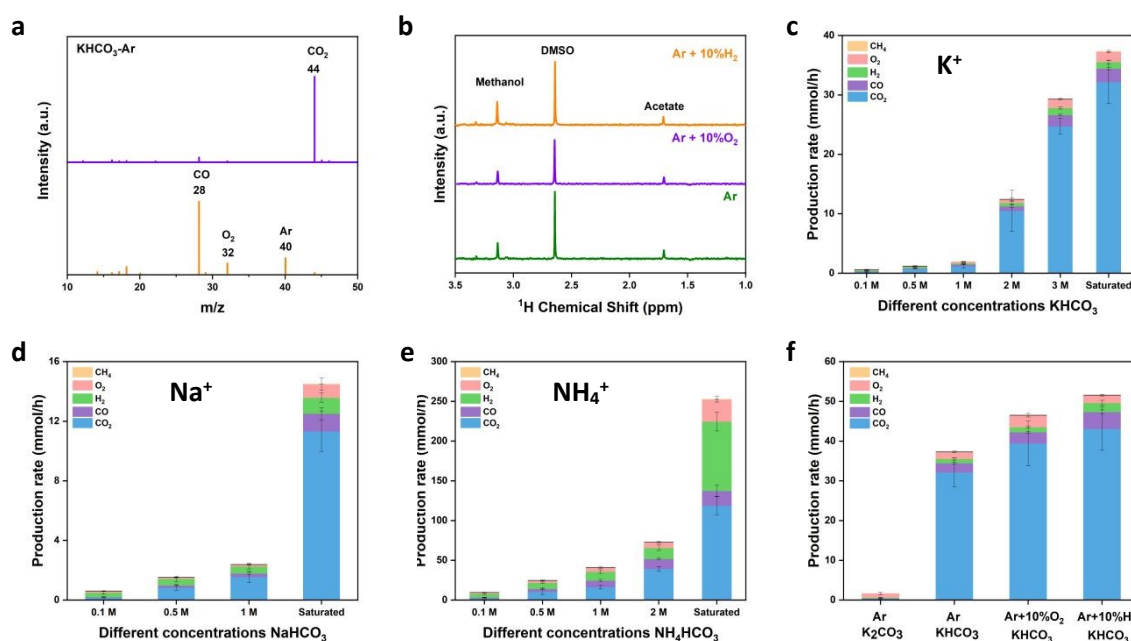


**Fig. 2.** (a) GC-MS spectra of plasma gas products under Ar with saturated  $\text{KHCO}_3$  solutions. (b)  $^1\text{H}$  NMR of plasma gas products under different carrier gases with saturated  $\text{KHCO}_3$  solutions. (c) Gas production rates under Ar with different  $\text{KHCO}_3$  concentrations. (d) Gas production rates under Ar with different  $\text{NaHCO}_3$  concentrations. (e) Gas production rates under Ar with different  $\text{NH}_4\text{HCO}_3$  concentrations. (f) Gas production rates under different carrier gases with saturated  $\text{KHCO}_3$  and  $\text{K}_2\text{CO}_3$ .





and acetate were identified (Fig. 2b). However, methanol and acetate stay in the bicarbonate solution bottle and do not participate in the subsequent electrochemical reaction.

Fig. S11 shows the time-dependent production rates of  $H_2$ ,  $O_2$ ,  $CH_4$ , and  $CO$  species, which exhibit excellent stability. This results confirm that the plasma reactor is highly stable for continuously operation.

Isotopically labelled H, C and O experiments were conducted to identify the source of H, C and O. To identify the H source, for the electrochemically generated  $CH_4$  and  $C_2H_4$ , we performed  $D_2O$ -labeling experiments by replacing the catholyte ( $KOH+H_2O$ ) with  $KOH+D_2O$  in the electrochemical reactor. As shown in Fig. S4, almost exclusive  $CD_4$  ( $m/z = 20$ ) and  $C_2D_4$  ( $m/z = 32$ ) are detected in GC/MS, suggesting that the H source comes from water in the electrolyte rather than from the plasma-generated  $H_2$ . To determine the source of carbon in our products, we conducted  $^{13}C$ -labeling experiments using  $NaH^{18}CO_3$  as the electrolyte in the plasma reactor. As shown in Fig. S5a, only  $^{13}CO_2$  ( $m/z = 45$ ) is detected in the mass spectra, confirming that the C source is derived from  $HCO_3^-$  and ruling out any potential carbon contamination. To identify the O source in  $CO_2$ , we conducted  $^{18}O$ -labeling experiments using  $H_2^{18}O$  in the plasma reactor. As shown in Fig. S5b, the mass spectra reveal the presence of a mixture of  $C^{16}O_2$  ( $m/z=44$ ),  $C^{18}O^{16}O$  ( $m/z=46$ ), and  $C^{18}O_2$  ( $m/z=48$ ), indicating that the O in  $CO_2$  originates from both  $HCO_3^-$  and  $H_2O$ . This is consistent with the expectation that both bicarbonate and water molecules are broken up during plasma.

Since the plasma discharge can interact with bicarbonate molecules either in the solution or the gas vapor phase, we first set out to investigate the impacts of different solutions and carrier gas conditions on the bicarbonate activation under the plasma field. In the solution phase, we examine the  $HCO_3^-$

solution with different cations,  $K^+$ ,  $Na^+$ , and  $NH_4^+$ , and quantify the respective plasma gas products. The yield of different species generated in the plasma reactor was quantified by GC at various concentrations of  $KHCO_3$ ,  $NaHCO_3$ , and  $NH_4HCO_3$ , illustrated in Fig. 2c-e. Under identical concentration conditions, the decomposition rate of  $HCO_3^-$  solution generally follows the trend of  $NH_4HCO_3 > NaHCO_3 > KHCO_3$ . If the salt concentrations are increased further, maximum production of  $CO_2$  is reached in the saturated form of each solution. Of particular interest to note is that the decomposition rate of  $NH_4HCO_3$  is orders of magnitude larger than  $NaHCO_3$  and  $KHCO_3$ . The reported thermal decomposition temperatures of  $KHCO_3$  and  $NaHCO_3$  are well over  $100^\circ C$ ,<sup>24, 25</sup> whereas the thermal decomposition temperature of  $NH_4HCO_3$  is reported at ca.  $30^\circ C$ .<sup>26</sup> Thus, the gas produced from plasma-activated  $NH_4HCO_3$  has a large contribution from thermal decomposition. We conducted control experiments to determine the contribution of thermal decomposition in  $KHCO_3$  and  $NaHCO_3$ . Fig. S9 demonstrates that only  $CO_2$  was produced when heating a  $NaHCO_3$  solution to  $80^\circ C$ , with a production rate reaching less than 20% of that achieved via plasma activation. This suggests that  $CO_2$  produced from  $KHCO_3$  and  $NaHCO_3$  are predominantly caused by plasma and to a small extent by thermal decomposition due to local temperature increase. The difference in the  $HCO_3^-$  solution decomposition rate between  $Na^+$  vs.  $K^+$  may be attributed to the change in the solution dielectric constant due to cation disruption to the water network.<sup>27</sup>

To further evaluate the  $HCO_3^-$  activation mechanism, electron spin resonance (EPR) was conducted to probe the formation of plasma-generated radicals and to evaluate the relationship between different cations and radical generations. 2,2,6,6-Tetramethylpiperidine 1-oxyl (TEMPO) was used as a

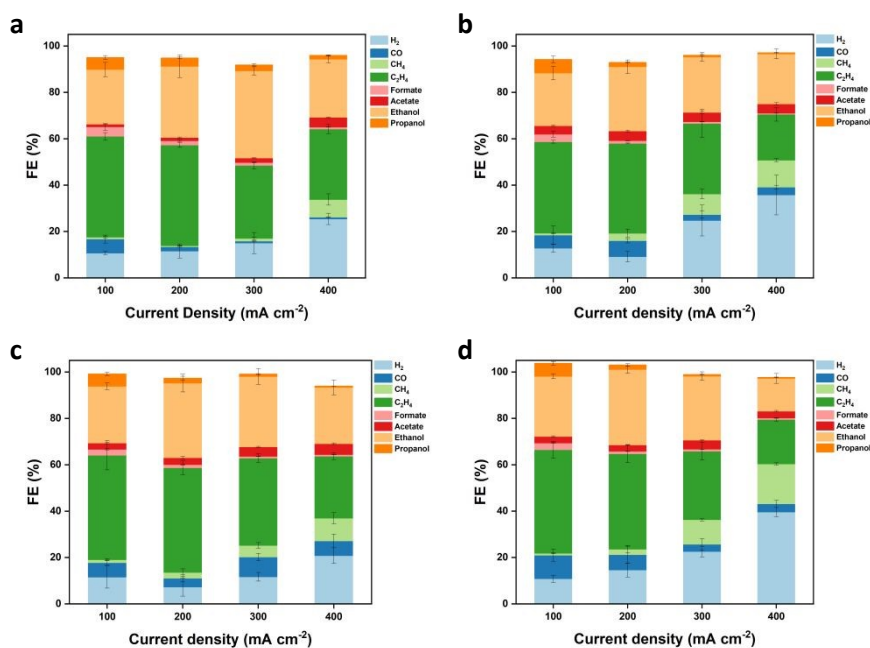


**Fig. 3.** The  $CO_2RR$  FE of a sputtered Cu catalyst under different conditions. (a) Pure  $CO_2$ . (b) Plasma-generated gases with Ar. (c) Plasma-generated gases with Ar + 10%  $H_2$ . (d) Plasma-generated gases with Ar + 10%  $O_2$ .



radical scavenger in the solution during plasma reaction, the amount of TEMPO consumed is a relative indication of the radicals generated during plasma. As shown in Fig. S10, the TEMPO concentration in EPR follows a trend of  $\text{NH}_4^+ < \text{K}^+ < \text{Na}^+$ , indicating that the  $\text{NH}_4\text{HCO}_3$  solution promotes the highest level of radical generation under plasma conditions, followed by  $\text{K}^+$  and  $\text{Na}^+$ . This trend is consistent with the production rates of plasma-generated gaseous products in Fig. 2 and confirms the impact of cation in solution.

The solubilities of  $\text{KHCO}_3$ ,  $\text{NaHCO}_3$ , and  $\text{NH}_4\text{HCO}_3$  at room temperature are 3.3 M, 1.2 M, and 2.7 M, respectively. Thus, under saturated concentrations, the bicarbonate activation rate of  $\text{KHCO}_3$  surpasses that of  $\text{NaHCO}_3$ . As shown in Tables S1 and S2, the saturated  $\text{NH}_4\text{HCO}_3$  solution produced a higher amount of CO and  $\text{CO}_2$  (137.38 mmol/h) compared to saturated  $\text{NaHCO}_3$  and  $\text{KHCO}_3$ , but at the same time, it also produces a significant amount of hydrogen, reaching 33.1 vol% of the final gas outlet. The CO plus  $\text{CO}_2$  concentration in the plasma reactor outlet was highest with saturated  $\text{KHCO}_3$  at 92.4 vol% of the total gas produced without carrier gas, and 69.3 vol% with carrier gas. Details on the gas production rates are provided in Table S2. Consequently, a saturated  $\text{KHCO}_3$  solution was selected as the carbon source for plasma activation in all subsequent experiments.

To investigate the gas-phase bicarbonate activation, we explored the effect of different carrier gases (Fig. 2f). Ar was originally chosen as a carrier gas due to its inertness. In this study, we introduce 10 %  $\text{H}_2$  and  $\text{O}_2$  gases into the plasma reactor with Ar, as two general reducing and oxidizing reactants to tune the outcome of the plasma products. The gaseous species observed under Ar with 10%  $\text{O}_2$  and Ar with 10%  $\text{H}_2$  were

similar to those detected under pure Ar. However, the production rates varied significantly. Especially, the production rate of  $\text{CO}_2$  (Table S3) under Ar with 10%  $\text{H}_2$  approached 43.11 mmol/h, which is 34% higher than pure Ar. The amount of CO and  $\text{H}_2$  was also higher than the Ar baseline. The CO plus  $\text{CO}_2$  concentration in the outlet of the plasma reactor with saturated  $\text{KHCO}_3$  under Ar with 10%  $\text{H}_2$  (Table S4) reached a maximum of 73.5 vol% with carrier gas. The addition of  $\text{H}_2$  in the plasma gas stream likely stabilizes the  $\text{OH}^-$  product from the dissociation of bicarbonate ( $\text{HCO}_3^- \rightarrow \text{CO}_2 + \text{OH}^-$ ), thus promoting the overall bicarbonate activation and  $\text{CO}_2$  production. The activation of carbonate solution under Ar was also tested under similar plasma conditions, however, the  $\text{CO}_2$  production rate is much lower than that of saturated  $\text{KHCO}_3$  solution, likely due to the higher stability of  $\text{K}_2\text{CO}_3$ .

As demonstrated by the results thus far, bicarbonate ions can be effectively activated into  $\text{CO}_2$  by plasma activation. Given these findings, we conducted a  $\text{CO}_2\text{RR}$  experiment using a Cu-PTFE catalyst in a flow cell setting with 1 M KOH electrolyte. Cu was chosen as it is the only catalyst effective toward  $\text{C}_{2+}$  products.<sup>28-31</sup> A baseline  $\text{CO}_2\text{RR}$  was first established using pure  $\text{CO}_2$  from gas cylinder to confirm the Cu catalyst product distribution in control conditions. As illustrated in Fig. 3a, the Cu-PTFE catalyst exhibited high  $\text{CO}_2\text{RR}$  selectivity while suppressing the competitive HER. At current densities of  $-100$ ,  $-200$ ,  $-300$ , and  $-400 \text{ mA cm}^{-2}$ , the  $\text{C}_{2+}$  products FEs were 73.5%, 79.5%, 73.6%, and 61.4%, respectively, consistent with prior reports.<sup>32, 33</sup> Subsequently, the plasma-activated  $\text{CO}_2$  was connected directly to the flow cell without any treatment and its performance is shown in Fig. S12. However, under this condition,  $\text{CH}_4$  and  $\text{H}_2$  were detected as major products. We

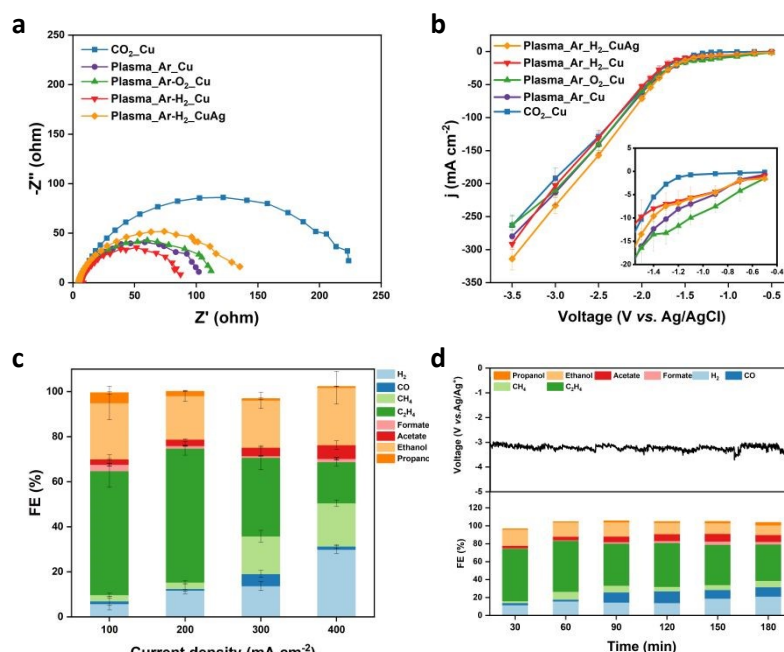


**Fig. 4.** (a) EIS spectra for the different  $\text{CO}_2\text{RR}$  conditions. (b)  $j$ -V curves for different  $\text{CO}_2\text{RR}$  conditions in the voltage range of  $-0.5 \sim -3.5 \text{ V}$  vs. Ag/AgCl, with the insert showing the enlarged  $j$ -V curves in the voltage range of  $-0.5 \sim -1.5 \text{ V}$  vs. Ag/AgCl. (c) The FE for plasma-generated  $\text{CO}_2$  with 90% Ar + 10%  $\text{H}_2$  carrier gases and CuAg alloy prepared by galvanic replacement reaction. (d) The stability test for the plasma-electrochemical configuration.



posit that the water content in the plasma products participated in the reduction reaction directly leading to hydrogen evolution. Additionally, excess water content reduced the CO<sub>2</sub> concentration, leading to CH<sub>4</sub> production, as suggested by previous reports on CO<sub>2</sub> concentration effects.<sup>34, 35</sup>

To mitigate the impacts of water, we reevaluate the CO<sub>2</sub>RR with a drierite column between the plasma and the electrochemical reaction, with results shown in, Fig. 3b. A maximum of 72.6% FE towards C<sub>2+</sub> at -200 mA cm<sup>-2</sup>, within standard deviation error to the control pure CO<sub>2</sub> (Fig. 3a). The small difference in performance may be due to the trace amount of water left in the gas stream. With the 10% H<sub>2</sub> in Ar carrier gas from the plasma reactor, the C<sub>2+</sub> FE increased further to 82.6% at -200 mA cm<sup>-2</sup> (Fig. 3d). The improvement is likely due to the presence of CO in the gas stream, which is a key intermediate during CO<sub>2</sub>RR towards C<sub>2+</sub> products. The FE performance of our plasma-electrochemical system matched or exceeded that of the baseline CO<sub>2</sub>RR FE obtained with pure CO<sub>2</sub>. It is also one of the best performances for direct bicarbonate conversion to ethylene in a CO<sub>2</sub> electrolyzer.

To eliminate concerns that plasma-generated methanol and acetate may evaporate and dissolve into the catholyte to influence the accuracy of CO<sub>2</sub>RR FE, we conducted a controlled experiment by running our plasma-electrochemical system for 30 minutes without applying any current/voltage to the electrochemical cell. The catholyte was then collected and analyzed by <sup>1</sup>H NMR. As shown in Fig. S13, when there is no electrochemical reaction, no detectable methanol or acetate signals were observed.

To probe the reaction kinetics, electrochemical impedance spectroscopy (EIS) was applied to investigate the kinetic differences between plasma-activated bicarbonate vs. pure CO<sub>2</sub> gas-fed electrolyzers. As demonstrated in Fig. 4a, the R<sub>s</sub> values across all conditions were similar within experimental errors. However, all plasma-activated conditions exhibited significantly lower charge transfer resistances (R<sub>ct</sub>) compared to pure CO<sub>2</sub>-fed conditions, indicating that the presence of mixed gases has enhanced the reaction kinetics. The fitted parameters and the equivalent circuit model for the EIS curves are provided in Table S6. The j-V curves for all conditions are shown in Fig. 4b. All voltages reported here are half-cell voltages versus the Ag/AgCl reference electrode without iR correction. Compared to the CO<sub>2</sub>-fed condition, plasma-activated systems exhibited a positive shift in onset potential from -1.1 V to -0.7 V (insert in Fig. 4b), indicating favorable reaction kinetics similar to the EIS results. This is likely contributed from the additional of CO in the gas stream, as CO<sub>2</sub> conversion to CO is often considered the rate limiting step.<sup>36</sup>

As illustrated in the electrochemical results, the abundance of CO\* and CO-related intermediates can effectively enhance CO<sub>2</sub>RR toward C<sub>2+</sub> products. Alloying Cu with CO-selective metals (e.g., Au, Ag, Zn) has been demonstrated to facilitate a sequential CO<sub>2</sub>-to-CO conversion for more efficient C-C coupling.<sup>37-40</sup> To further enhance FE for C<sub>2+</sub> products, a CuAg bimetallic alloy was prepared via the galvanic substitution method. Representative scanning electron microscopy (SEM) and energy-dispersive X-ray spectroscopic (EDS) images (Fig.

S14-15) confirmed the homogeneous distribution of Cu and Ag in Cu-PTFE and CuAg-PTFE catalysts. X-ray photoelectron spectroscopy (XPS) provided further insight into the composition and electronic structure of synthesized Cu-PTFE and CuAg-PTFE. The Cu 2p spectra of Cu-PTFE (Fig. S16) exhibited two major peaks at 933.2 eV and 952.0 eV with a 2:1 area ratio, representing Cu 2p<sub>3/2</sub> and Cu 2p<sub>1/2</sub>. The peaks at 934.4 eV and 955.2 eV were ascribed to Cu<sup>2+</sup> species. These oxidized species were formed due to air exposure, which will be reduced to the metallic states under our electrochemical process. After alloying with Ag, the Cu 2p spectra (Fig. S17a) exhibited a positive shift, indicating altered surface electronic states. The Ag 3d XPS spectra (Fig. S17b) of CuAg-PTFE revealed peaks at 367.8 eV and 373.8 eV, corresponding to Ag 3d<sub>5/2</sub> and Ag 3d<sub>3/2</sub>, respectively. Fig. 4c demonstrated the CO<sub>2</sub>RR FE for the CuAg-PTFE, achieving a C<sub>2+</sub> FE of 83.7% at a current density of -200 mA cm<sup>-2</sup> with C<sub>2</sub>H<sub>4</sub> as the dominant product, reaching a selectivity of 59.5%. To evaluate the overall plasma-electrochemical system stability, a constant current experiment at -200 mA cm<sup>-2</sup> was conducted with gas products from the plasma reactor. Gas and liquid products from CO<sub>2</sub>RR were collected every 30 minutes for product analysis. As illustrated in Fig. 4d, the system maintained a C<sub>2+</sub> FE of 62.3% after 180 minutes, demonstrating good operational stability. For Comparison, we compiled recent reports on direct bicarbonate to C<sub>2+</sub> conversion in Table S7. Notably, our plasma-activated bicarbonate method achieves the highest FE for C<sub>2+</sub> products.<sup>41-48</sup> At the same time, we do acknowledge that our current energy efficiency is not sufficiently impactful and it is an area of improvement that we are actively working on.

## 4. Conclusions

The current work demonstrates a hybrid plasma-electrochemical system to enable the ex-situ activation of the bicarbonate solutions and optimization of the gas-phase composition for electrochemical CO<sub>2</sub> reduction. This approach provides an alternative route for direct bicarbonate conversion to value-added products compared to a BPM-based electrolyzer. The CO<sub>2</sub>-to-C<sub>2+</sub> selectivity is enhanced due to the CO addition to the CO<sub>2</sub> stream, promoting C-C coupling. Under optimized plasma conditions with saturated KHCO<sub>3</sub> and Ar + 10% H<sub>2</sub>, a maximum CO/CO<sub>2</sub> concentration of 73.5 % was achieved in the plasma reactor output. When coupled with a CO-selective CuAg-PTFE catalyst, the continuous plasma-electrochemical system realized a record C<sub>2+</sub> FE of 83.7% at -200 mA cm<sup>-2</sup> with C<sub>2</sub>H<sub>4</sub> selectivity reaching 59.5%. This plasma electrochemical system can provide utilities beyond CO<sub>2</sub> reduction to facilitate the electrochemical synthesis of otherwise difficult-to-activate species, such as CH<sub>4</sub>, N<sub>2</sub>, or polymeric compounds, providing a new pathway to realize a carbon-neutral economy.

## Author contributions





Y.C.L. and X.G. conceptualize the idea of this project. The manuscript was written through contributions of all authors. All authors have given approval of the final version of the manuscript.

## Conflicts of interest

There are no conflicts to declare.

## Data availability

The data that support this study are available within the article and its supplementary information.

Supplementary information is available. See DOI: XXX

## Acknowledgements

Y.C.L would like to thank the Research Corporation for Science Advancement for funding support through the Cottrell Scholar Award.

## References

- W. Lai, Z. Ma, J. Zhang, Y. Yuan, Y. Qiao and H. Huang, *Advanced Functional Materials*, 2022, **32**, 2111193.
- W. Lai, Y. Qiao, J. Zhang, Z. Lin and H. Huang, *Energy & Environmental Science*, 2022, **15**, 3603-3629.
- S. Jin, Z. Hao, K. Zhang, Z. Yan and J. Chen, *Angewandte Chemie*, 2021, **133**, 20795-20816.
- D. W. Keith, G. Holmes, D. S. Angelo and K. Heidel, *Joule*, 2018, **2**, 1573-1594.
- J. E. Huang, F. Li, A. Ozden, A. Sedighian Rasouli, F. P. García de Arquer, S. Liu, S. Zhang, M. Luo, X. Wang and Y. Lum, *Science*, 2021, **372**, 1074-1078.
- S. Liu, J. Zhang, F. Li, J. P. Edwards, Y. C. Xiao, D. Kim, P. Papangelakis, J. Kim, D. Elder and P. De Luna, *Energy & Environmental Science*, 2024, **17**, 1266-1278.
- D. J. Pimlott, Y. Kim and C. P. Berlinguette, *Accounts of Chemical Research*, 2024, **57**, 1007-1018.
- Q. Xia, K. Zhang, T. Zheng, L. An, C. Xia and X. Zhang, *ACS Energy Letters*, 2023, **8**, 2840-2857.
- A. Ozden, F. P. García de Arquer, J. E. Huang, J. Wicks, J. Sisler, R. K. Miao, C. P. O'Brien, G. Lee, X. Wang and A. H. Ip, *Nature Sustainability*, 2022, **5**, 563-573.
- Y. C. Li, G. Lee, T. Yuan, Y. Wang, D.-H. Nam, Z. Wang, F. P. García de Arquer, Y. Lum, C.-T. Dinh and O. Voznyy, *ACS Energy Lett.*, 2019, **4**, 1427-1431.
- G. Lee, A. S. Rasouli, B.-H. Lee, J. Zhang, Y. C. Xiao, J. P. Edwards, M. G. Lee, E. D. Jung, F. Arabymohammadi and H. Liu, *Joule*, 2023, **7**, 1277-1288.
- H. Song, C. A. Fernández, H. Choi, P.-W. Huang, J. Oh and M. C. Hatzell, *Energy & Environmental Science*, 2024, **17**, 3570-3579.
- Z. Zhang, D. Xi, Z. Ren and J. Li, *Cell Reports Physical Science*, 2023, **4**, 101662.
- A. George, B. Shen, M. Craven, Y. Wang, D. Kang, C. Wu and X. Tu, *Renewable and Sustainable Energy Reviews*, 2021, **135**, 109702.
- J. Knezevic, T. Zhang, R. Zhou, J. Hong, R. Zhou, C. Barnett, Q. Song, Y. Gao, W. Xu and D. Liu, *Journal of the American Chemical Society*, 2024, **146**, 12601-12608.
- X. Ge, C. Zhang, M. Janpandit, S. Prakash, P. Gogoi, D. Zhang, T. R. Cook, G. I. Waterhouse, L. Yin and Z. Wang, *Journal of the American Chemical Society*, 2024, **146**, 35305-35312.
- L. Dou, Y. Liu, Y. Gao, J. Li, X. Hu, S. Zhang, K. K. Ostrikov and T. Shao, *Applied Catalysis B: Environmental*, 2022, **318**, 121830.
- N. Joshi and S. Loganathan, *ACS omega*, 2023, **8**, 13410-13420.
- C. De Bie, J. van Dijk and A. Bogaerts, *The Journal of Physical Chemistry C*, 2016, **120**, 25210-25224.
- S. Meng, L. Wu, M. Liu, Z. Cui, Q. Chen, S. Li, J. Yan, L. Wang, X. Wang and J. Qian, *AIChE Journal*, 2023, **69**, e18154.
- H. Zeghioud, P. Nguyen-Tri, L. Khezami, A. Amrane and A. A. Assadi, *J. Water Process Eng.*, 2020, **38**, 101664.
- C. A. Aggelopoulos, *Chem. Eng. J.*, 2022, **428**, 131657.
- G. T. Bae, J. Y. Kim, D. Y. Kim, E. Y. Jung, H. J. Jang, C.-S. Park, H. Jang, D. H. Lee, H.-K. Lee and H.-S. Tae, *Materials*, 2021, **14**, 7559.
- M. Hartman, K. Svoboda, B. r. Čech, M. Pohořelý and M. Šyc, *Ind. Eng. Chem. Res.*, 2019, **58**, 2868-2881.
- R. S. Gärtner, M. M. Seckler and G.-J. Witkamp, *Ind. Eng. Chem. Res.*, 2005, **44**, 4272-4283.
- P. Nowak and J. Skrzypek, *Chem. Eng. Sci.*, 1989, **44**, 2375.
- G. Das, S. Hlushak, M. C. Dos Ramos and C. McCabe, *AIChE Journal*, 2015, **61**, 3053-3072.
- D. Raciti and C. Wang, *ACS Energy Letters*, 2018, **3**, 1545-1556.
- G. L. De Gregorio, T. Burdyny, A. Loiudice, P. Iyengar, W. A. Smith and R. Buonsanti, *ACS catalysis*, 2020, **10**, 4854-4862.
- F. Li, Y. C. Li, Z. Wang, J. Li, D.-H. Nam, Y. Lum, M. Luo, X. Wang, A. Ozden and S.-F. Hung, *Nature Catalysis*, 2020, **3**, 75-82.
- Y. C. Li, Z. Wang, T. Yuan, D.-H. Nam, M. Luo, J. Wicks, B. Chen, J. Li, F. Li and F. P. G. De Arquer, *Journal of the American Chemical Society*, 2019, **141**, 8584-8591.
- Z. Wang, Y. Li, X. Zhao, S. Chen, Q. Nian, X. Luo, J. Fan, D. Ruan, B.-Q. Xiong and X. Ren, *Journal of the American Chemical Society*, 2023, **145**, 6339-6348.
- M. Luo, Z. Wang, Y. C. Li, J. Li, F. Li, Y. Lum, D.-H. Nam, B. Chen, J. Wicks and A. Xu, *Nature communications*, 2019, **10**, 5814.
- C. Deacon-Price, N. Chen, A. Lal, P. Broersen, E. J. Meijer and A. C. Garcia, *ChemCatChem*, 2025, e202401332.
- X. Wang, A. Xu, F. Li, S.-F. Hung, D.-H. Nam, C. M. Gabardo, Z. Wang, Y. Xu, A. Ozden and A. S. Rasouli, *J. Am. Chem. Soc.*, 2020, **142**, 3525-3531.
- W. Ma, X. He, W. Wang, S. Xie, Q. Zhang and Y. Wang, *Chem. Soc. Rev.*, 2021, **50**, 12897-12914.
- C. Chen, Y. Li, S. Yu, S. Louisia, J. Jin, M. Li, M. B. Ross and P. Yang, *Joule*, 2020, **4**, 1688-1699.
- F. A. Rollier, V. Muravev, N. Kosinov, T. Wissink, D. Anastasiadou, B. Ligt, L. Barthe, M. C. Figueiredo and E. J. Hensen, *Journal of Materials Chemistry A*, 2025, **13**, 2285-2300.
- P. Guo, K. Liu, X. Liu, R. Liu and Z. Yin, *Energy & Fuels*, 2024, **38**, 5659-5675.



## ARTICLE

## Journal Name

40. A. Vasileff, C. Xu, Y. Jiao, Y. Zheng and S.-Z. Qiao, *Chem*, 2018, **4**, 1809-1831.
41. G. Lee, A. S. Rasouli, B.-H. Lee, J. Zhang, D. H. Won, Y. C. Xiao, J. P. Edwards, M. G. Lee, E. D. Jung and F. Arabyarmohammadi, *Joule*, 2023, **7**, 1277-1288.
42. S. Ma, Y. Kim, Z. Zhang, S. Ren, C. Donde, L. Melo, A. S. Williams, M. Stolar, E. R. Grant and C. P. Berlinguette, *ACS Energy Letters*, 2024, **9**, 2326-2332.
43. Y. C. Li, G. Lee, T. Yuan, Y. Wang, D.-H. Nam, Z. Wang, F. P. García de Arquer, Y. Lum, C.-T. Dinh and O. Voznyy, *ACS Energy Letters*, 2019, **4**, 1427-1431.
44. H. Song, C. A. Fernández, A. Venkataraman, V. D. Brandão, S. S. Dhingra, S. S. Arora, S. S. Bhargava, C. M. Villa, C. Sievers and S. Nair, *ACS Applied Energy Materials*, 2024, **7**, 1224-1233.
45. J. Lee, H. Liu and W. Li, *ChemSusChem*, 2022, **15**, e202201329.
46. B. N. Khiarak, G. T. da Silva, J. Crane, C. P. O'Brien, M. R. Pepe, C. M. Gabardo, V. Golovanova, F. P. García de Arquer and C. T. Dinh, *Angewandte Chemie*, 2025, **137**, e202509975.
47. J. Wang, Z. Zhang, W. Wu, Y. Liu, B. Dong, Y. Wang and Y. Wang, *ACS Energy Letters*, 2023, **9**, 110-117.
48. S. Ma, H. Hu, F. Shen, Z. Chen and J. Hu, *Small*, e11008.

View Article Online  
DOI: 10.1039/D5GC05361G



The data that support this study are available within the article and its supplementary information.  
Supplementary information is available. See DOI: XXX

